

We are IntechOpen, the world's leading publisher of Open Access books Built by scientists, for scientists

6,900

Open access books available

186,000

International authors and editors

200M

Downloads

Our authors are among the

154

Countries delivered to

TOP 1%

most cited scientists

12.2%

Contributors from top 500 universities



WEB OF SCIENCE™

Selection of our books indexed in the Book Citation Index
in Web of Science™ Core Collection (BKCI)

Interested in publishing with us?
Contact book.department@intechopen.com

Numbers displayed above are based on latest data collected.
For more information visit www.intechopen.com



Zero and Low-Speed Sensorless Control of Induction Machines Using Only Fundamental Pulse Width Modulation Waveform Excitation

Qiang Gao, Greg Asher and Mark Sumner

Additional information is available at the end of the chapter

<http://dx.doi.org/10.5772/intechopen.75892>

Abstract

This chapter presents a position sensorless method for induction machines that only relies on the fundamental pulse width modulation (PWM) waveforms to excite saliency. Position signals can be synthesized through the measurement of the derivatives of the line currents induced by the PWM voltage vectors. This method is essentially saliency detection based, and therefore derivation of the rotor position is possible at low and zero speeds. In addition, it works also at higher speeds without the need of the knowledge of the machine's fundamental model. Experimental results showing fully sensorless induction motor control at low and higher speeds validate the principle of this method.

Keywords: sensorless control, induction machine, saliency, PWM excitation, current derivative

1. Introduction

Due to the incapacity of the fundamental model-based sensorless rotor position estimation at zero and low frequencies, alternative methods have been intensively studied. These methods exploit the anisotropy or saliency of the machine resulting from either saturation or geometric variation on the rotor. They can be classified into two categories according to the detection method for the anisotropy (or saliency) position. One category relies on the continuous injection of high-frequency voltage signals and then measuring the response of the high-frequency (*hf*) current [1–7]. Demodulation of the *hf* current signal enables the extraction of the rotor angle. The second category makes use of the line-current transient response to a PWM switching state. This can be realized by injecting special voltage test vectors [8–13] or by modifying the normal pulse width modulation waveforms

[14], which may increase the hazardous common mode current in the machine [15]. The induced current transient response during a test vector reflects the spatial variation of the stator leakage inductances due to the anisotropy. Therefore, it is possible to acquire the rotor position, or rotor flux angle, through the measurement of the transient current derivative in response to the test vector.

In this chapter, a method belonging to the second category is described. Instead of using extra test vectors or modifying the standard modulation scheme, this method integrates the test vectors with the standard PWM waveforms [16]. In the following paragraphs, the theory of the method will be presented first, then, its application on a 4-pole 30 kW Δ -connected cage machine having 56 open slots will be demonstrated. Other implementation issues related to the speed sensorless operation, such as the noise filter of the position signals, will also be introduced.

2. Position estimation with the fundamental wave PWM

When a three-phase, delta-connected induction machine has its stator leakage inductances modulated by the anisotropies introduced by either the main flux saturation or the rotor slotting, they can be assumed to vary according to:

$$l_{\sigma a} = l_0 + \Delta l \cos(n_{an} \theta_{an}) \quad (1)$$

$$l_{\sigma b} = l_0 + \Delta l \cos(n_{an} (\theta_{an} - 2\pi/3)) \quad (2)$$

$$l_{\sigma c} = l_0 + \Delta l \cos(n_{an} (\theta_{an} - 4\pi/3)) \quad (3)$$

where l_0 is the average inductance and Δl is the amplitude of inductance variation caused by the anisotropy ($n_{an} = 2$ for saturation-induced anisotropy or $n_{an} = n_{rs} = N_r/p$ for rotor slotting, where N_r is rotor slot number and p the pole pairs).

The standard space vectors of **Figure 1** are applied. **Figure 2** shows the equivalent circuit when the machine is applied with vector \underline{u}_1 from which the following equations can be derived:

$$U_d = i_{ab}^{(u1)} r_s + l_{\sigma a} \frac{di_{ab}^{(u1)}}{dt} + e_a^{(u1)} \quad (4)$$

$$0 = i_{bc}^{(u1)} r_s + l_{\sigma b} \frac{di_{bc}^{(u1)}}{dt} + e_b^{(u1)} \quad (5)$$

$$-U_d = i_{ca}^{(u1)} r_s + l_{\sigma c} \frac{di_{ca}^{(u1)}}{dt} + e_c^{(u1)} \quad (6)$$

By the application of the null vector \underline{u}_0 or \underline{u}_7 , one has:

$$0 = i_{ab}^{(u0)} r_s + l_{\sigma a} \frac{di_{ab}^{(u0)}}{dt} + e_a^{(u0)} \quad (7)$$

$$0 = i_{bc}^{(u0)} r_s + l_{\sigma b} \frac{di_{bc}^{(u0)}}{dt} + e_b^{(u0)} \quad (8)$$

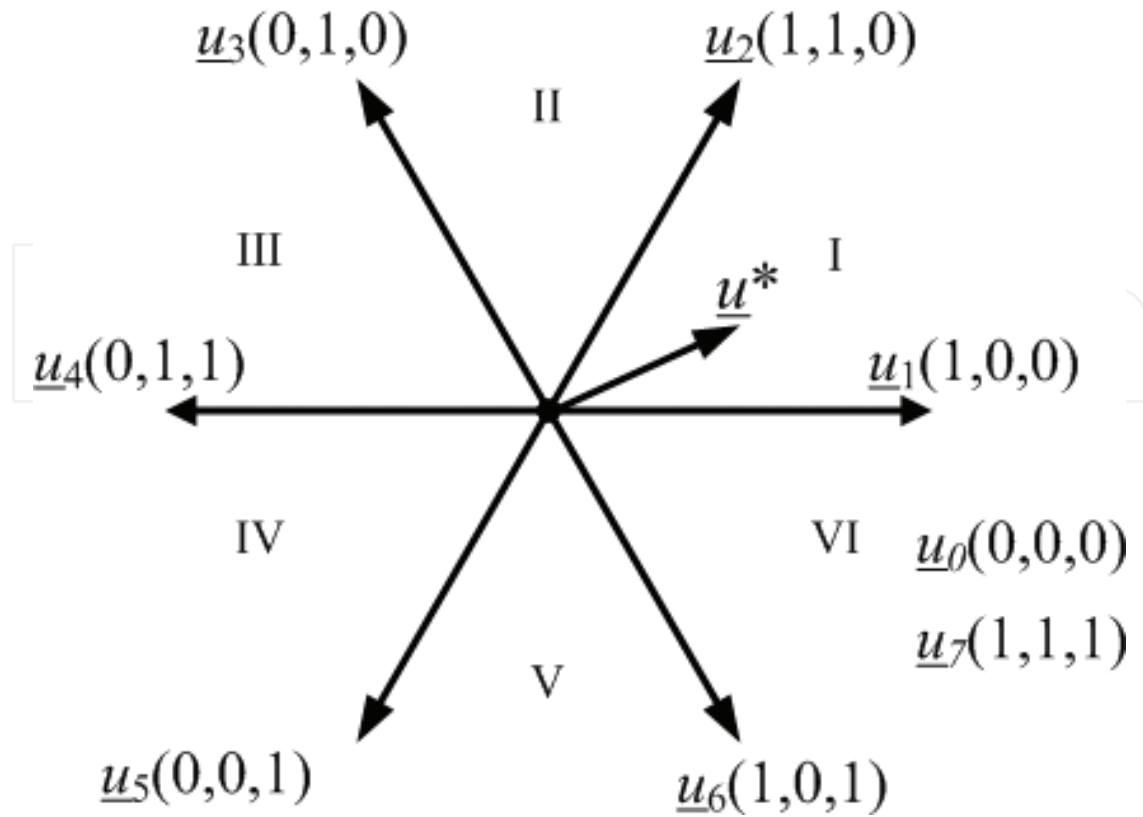


Figure 1. Definition of space vectors.

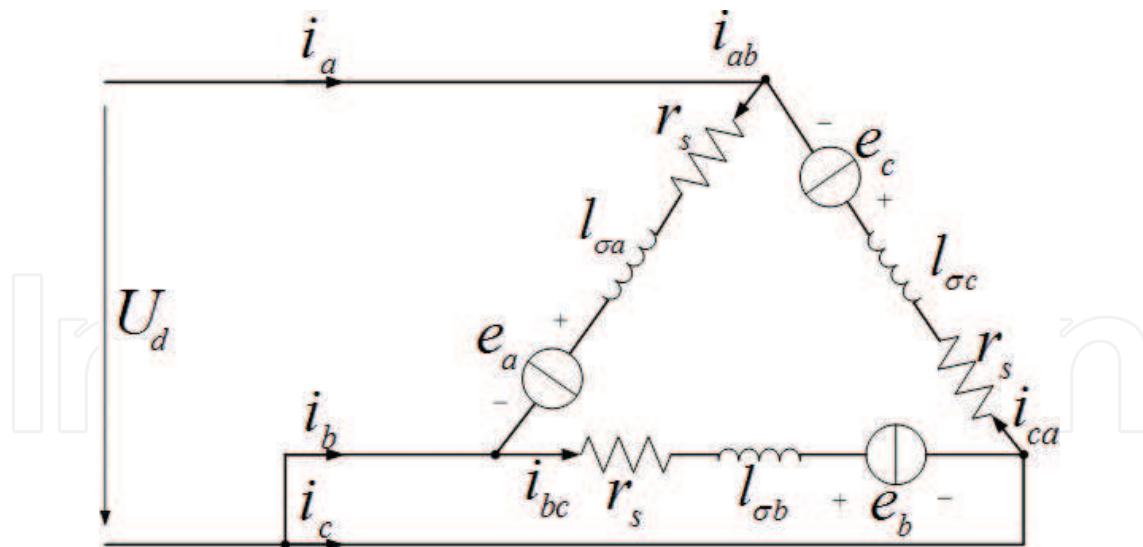


Figure 2. Equivalent circuit with \underline{u}_1 being applied.

$$0 = i_{ca}^{(u0)} r_s + l_{\sigma c} \frac{di_{ca}^{(u0)}}{dt} + e_c^{(u0)} \quad (9)$$

If the instants of applying \underline{u}_1 and \underline{u}_0 are close enough, it is viable to assume that:

$$e_a^{(u0)} \approx e_a^{(u1)}, e_b^{(u0)} \approx e_b^{(u1)}, e_c^{(u0)} \approx e_c^{(u1)}.$$

Additionally, the voltage drops across the stator resistance and can be ignored due to their small values compared with U_d .

Hence, the subtraction of the Eqs. (4)–(7), (5)–(8) and (6)–(9) yields:

$$\frac{di_{ab}^{(u1)}}{dt} - \frac{di_{ab}^{(u0)}}{dt} = \frac{U_d}{l_{\sigma a}} \quad (10)$$

$$\frac{di_{bc}^{(u1)}}{dt} - \frac{di_{bc}^{(u0)}}{dt} = 0 \quad (11)$$

$$\frac{di_{ca}^{(u1)}}{dt} - \frac{di_{ca}^{(u0)}}{dt} = -\frac{U_d}{l_{\sigma a}} \quad (12)$$

From the relationship between phase currents and line currents, for example, $i_a = i_{ab} - i_{ca}$, one has:

$$\frac{di_a^{(u1)}}{dt} - \frac{di_a^{(u0)}}{dt} = \frac{l_{\sigma a} + l_{\sigma c}}{l_{\sigma a} l_{\sigma c}} U_d \quad (13)$$

$$\frac{di_b^{(u1)}}{dt} - \frac{di_b^{(u0)}}{dt} = -\frac{1}{l_{\sigma a}} U_d \quad (14)$$

$$\frac{di_c^{(u1)}}{dt} - \frac{di_c^{(u0)}}{dt} = -\frac{1}{l_{\sigma c}} U_d \quad (15)$$

Considering Eqs. (1) to (3), one has:

$$\frac{di_a^{(u1)}}{dt} - \frac{di_a^{(u0)}}{dt} = \frac{U_d}{l_0} \left(2 + \frac{\Delta l}{l_0} \cos \left(n_{an} \left(\theta_{an} - \frac{2\pi}{3} \right) \right) \right) \quad (16)$$

$$\frac{di_b^{(u1)}}{dt} - \frac{di_b^{(u0)}}{dt} = -\frac{U_d}{l_0} \left(1 - \frac{\Delta l}{l_0} \cos(n_{an} \theta_{an}) \right) \quad (17)$$

$$\frac{di_c^{(u1)}}{dt} - \frac{di_c^{(u0)}}{dt} = -\frac{U_d}{l_0} \left(1 - \frac{\Delta l}{l_0} \cos \left(n_{an} \left(\theta_{an} - \frac{4\pi}{3} \right) \right) \right) \quad (18)$$

from which three balanced position scalars p_a , p_b and p_c can be defined as follows:

$$p_a = 1 + c_1 \left(\frac{di_b^{(u1)}}{dt} - \frac{di_b^{(u0)}}{dt} \right) \quad (19)$$

$$p_b = -2 + c_1 \left(\frac{di_a^{(u1)}}{dt} - \frac{di_a^{(u0)}}{dt} \right) \quad (20)$$

$$p_c = 1 + c_1 \left(\frac{di_c^{(u1)}}{dt} - \frac{di_c^{(u0)}}{dt} \right) \tag{21}$$

where $c_1 = l_0/U_d$. If both c_1 and $\frac{di}{dt}$ are known, it is possible to construct the position vector p directly via:

$$\underline{p} = p_a + a \cdot p_b + a^2 \cdot p_c \tag{22}$$

where $a = e^{j2\pi/3}$. However, c_1 consists of an unknown coefficient l_0 , which may vary with the saturation level of the main flux. This uncertainty can be avoided by looking at the current response to another voltage vector \underline{u}_2 . Following the same as earlier, another three position scalars can be defined as:

$$p_a = -2 - c_1 \left(\frac{di_c^{(u2)}}{dt} - \frac{di_c^{(u0)}}{dt} \right) \tag{23}$$

$$p_b = 1 - c_1 \left(\frac{di_b^{(u2)}}{dt} - \frac{di_b^{(u0)}}{dt} \right) \tag{24}$$

$$p_c = 1 - c_1 \left(\frac{di_a^{(u2)}}{dt} - \frac{di_a^{(u0)}}{dt} \right) \tag{25}$$

It should be noted that because the application of \underline{u}_1 and \underline{u}_2 results in the same position scalars, they are defined with the same terms, p_a , p_b and p_c .

By referring to (19), (20), (21) and (23), (24), (25), it is possible to define \underline{p} through the combination of (19), (24) and (25):

$$\begin{aligned} \underline{p} &= p_\alpha + jp_\beta = p_a + ap_b + a^2p_c \\ &= c_1 \left[\begin{array}{l} \left(\frac{di_b^{(u1)}}{dt} - \frac{di_b^{(u0)}}{dt} \right) - a \left(\frac{di_b^{(u2)}}{dt} - \frac{di_b^{(u0)}}{dt} \right) \\ -a^2 \left(\frac{di_a^{(u2)}}{dt} - \frac{di_a^{(u0)}}{dt} \right) \end{array} \right] \end{aligned} \tag{26}$$

Therefore,

$$p_\alpha = c_1 \left[\begin{array}{l} \left(\frac{di_b^{(u1)}}{dt} - \frac{di_b^{(u0)}}{dt} \right) + \frac{1}{2} \left(\frac{di_b^{(u2)}}{dt} - \frac{di_b^{(u0)}}{dt} \right) \\ + \frac{1}{2} \left(\frac{di_a^{(u2)}}{dt} - \frac{di_a^{(u0)}}{dt} \right) \end{array} \right] \tag{27}$$

	p_a	p_b	p_c
$\frac{\underline{U}_1}{\underline{U}_0}$	$1 + c_1 \left(\frac{di_b^{(u1)}}{dt} - \frac{di_b^{(u0)}}{dt} \right)$	$-2 + c_1 \left(\frac{di_a^{(u1)}}{dt} - \frac{di_a^{(u0)}}{dt} \right)$	$1 + c_1 \left(\frac{di_c^{(u1)}}{dt} - \frac{di_c^{(u0)}}{dt} \right)$
$\frac{\underline{U}_2}{\underline{U}_0}$	$-2 - c_1 \left(\frac{di_c^{(u2)}}{dt} - \frac{di_c^{(u0)}}{dt} \right)$	$1 - c_1 \left(\frac{di_b^{(u2)}}{dt} - \frac{di_b^{(u0)}}{dt} \right)$	$1 - c_1 \left(\frac{di_a^{(u2)}}{dt} - \frac{di_a^{(u0)}}{dt} \right)$
$\frac{\underline{U}_3}{\underline{U}_0}$	$1 + c_1 \left(\frac{di_a^{(u3)}}{dt} - \frac{di_a^{(u0)}}{dt} \right)$	$1 + c_1 \left(\frac{di_c^{(u3)}}{dt} - \frac{di_c^{(u0)}}{dt} \right)$	$-2 + c_1 \left(\frac{di_b^{(u3)}}{dt} - \frac{di_b^{(u0)}}{dt} \right)$
$\frac{\underline{U}_4}{\underline{U}_0}$	$1 - c_1 \left(\frac{di_b^{(u4)}}{dt} - \frac{di_b^{(u0)}}{dt} \right)$	$-2 - c_1 \left(\frac{di_a^{(u4)}}{dt} - \frac{di_a^{(u0)}}{dt} \right)$	$1 - c_1 \left(\frac{di_c^{(u4)}}{dt} - \frac{di_c^{(u0)}}{dt} \right)$
$\frac{\underline{U}_5}{\underline{U}_0}$	$-2 - c_1 \left(\frac{di_c^{(u5)}}{dt} - \frac{di_c^{(u0)}}{dt} \right)$	$1 + c_1 \left(\frac{di_b^{(u5)}}{dt} - \frac{di_b^{(u0)}}{dt} \right)$	$1 + c_1 \left(\frac{di_a^{(u5)}}{dt} - \frac{di_a^{(u0)}}{dt} \right)$
$\frac{\underline{U}_6}{\underline{U}_0}$	$1 - c_1 \left(\frac{di_a^{(u6)}}{dt} - \frac{di_a^{(u0)}}{dt} \right)$	$1 - c_1 \left(\frac{di_c^{(u6)}}{dt} - \frac{di_c^{(u0)}}{dt} \right)$	$-2 - c_1 \left(\frac{di_b^{(u6)}}{dt} - \frac{di_b^{(u0)}}{dt} \right)$

Table 1. Definition of position scalars of all voltage vectors in a delta-connected IM.

$$p_\beta = \frac{\sqrt{3}}{2} c_1 \left[\left(\frac{di_a^{(u2)}}{dt} - \frac{di_a^{(u0)}}{dt} \right) - \left(\frac{di_b^{(u2)}}{dt} - \frac{di_b^{(u0)}}{dt} \right) \right] \quad (28)$$

whereby the position can be derived through the arctan operation as shown in (29).

$$\theta_{an} = \arctan(p_\beta/p_\alpha) \quad (29)$$

Such a combination between two adjacent voltage vectors, and a null vector, also exists in other five sectors. Therefore, the position estimation is achievable using only the fundamental PWM sequence. **Table 1** gives the position scalars corresponding to all the vectors.

3. Experimental implementation

3.1. Practical considerations

It can be seen that the correct position estimation relies on the precise measurement of the di/dt signals. For this aim, air-cored Rogowski [9], ferrite-cored Rogowski [18], or air-cored coaxial cable-typed [14] transducers can be used. Or direct digital calculation, $di/dt = i(t_2) - i(t_1) / (t_2 - t_1)$, can be employed instead. **Figure 3** shows a typical di/dt signal along with ADC trigger signal when an air-cored coaxial cable-typed transducer is used.

Another important issue comes from the fact that due to the common/differential mode voltages produced by the inverter, high-frequency oscillation exists in the phase currents, which poses a challenge for accurate di/dt measurement. This is true when dwell times of the voltage vectors are too short or when the reference voltage vectors pass the boundaries of sectors. Therefore, a minimum dwell time, t_{min} , is imposed on voltage vectors for di/dt measurement. When the original dwell time of a voltage vector, t , is shorter than t_{min} , an opposite vector with a dwell time, $t_{min} - t$, is added to maintain the volt-second. This procedure can be realized simply by the edge-shifting technique, which is illustrated in **Figure 4** when the reference voltage lies in Sector I.

3.2. System schematic

Figure 5 shows the system schematic of the sensorless speed control. Three di/dt sensors are connected in series with the lines of the induction motor, whose parameters are given in **Table 2**. The position vector formation block synthesizes the position vector $p_{\alpha\beta}$ according to the measured di/dt s and the sector index (S_i) of the reference voltage vector. For example,

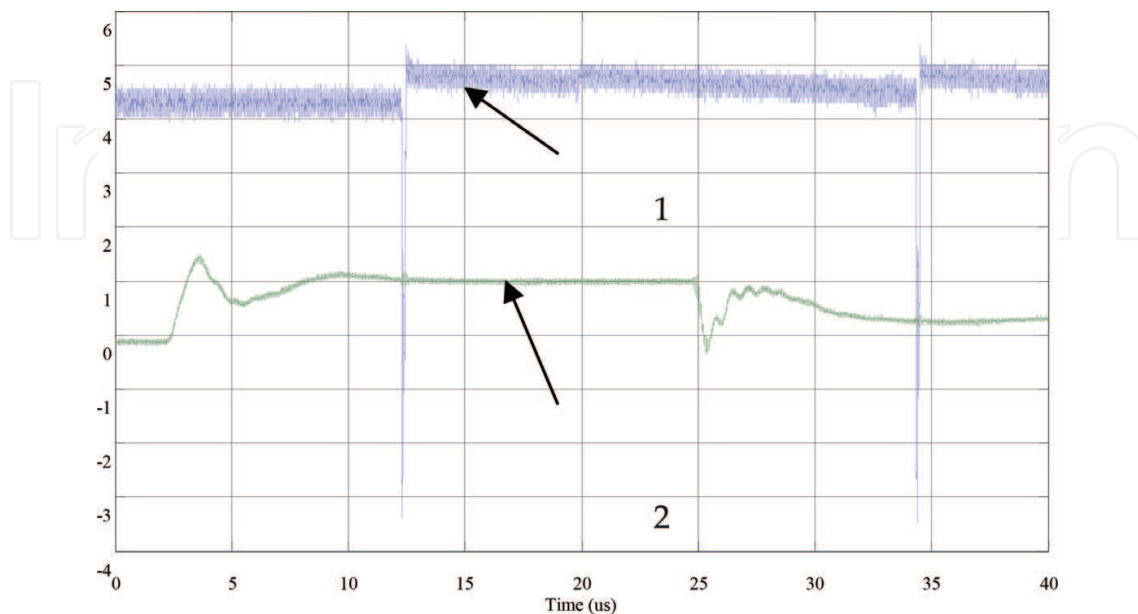


Figure 3. ADC trigger signal (1,V) and di/dt signal (2,V) measured by a air-cored coaxial cable type transducers.

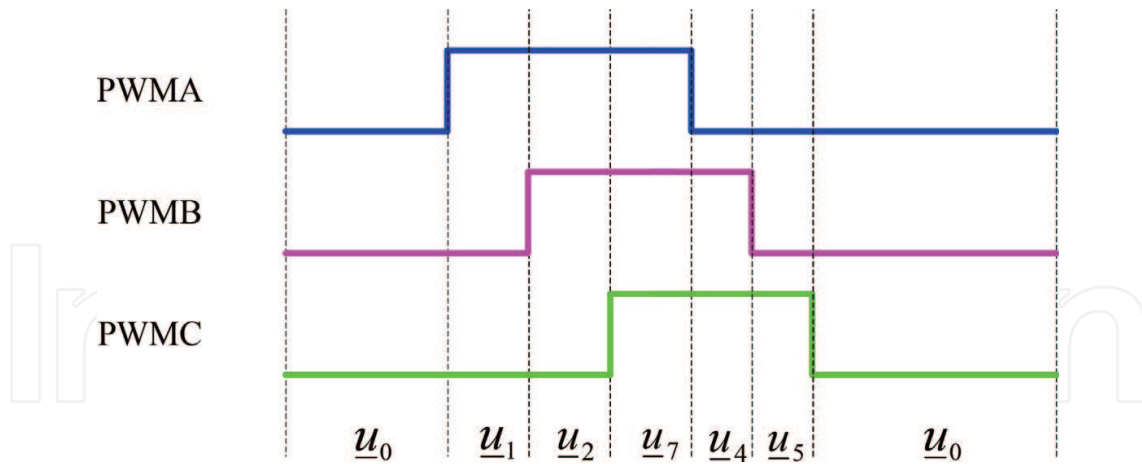


Figure 4. Edge shifting of PWM waveforms when the dwell times of u_1 and u_2 are smaller than t_{min} .

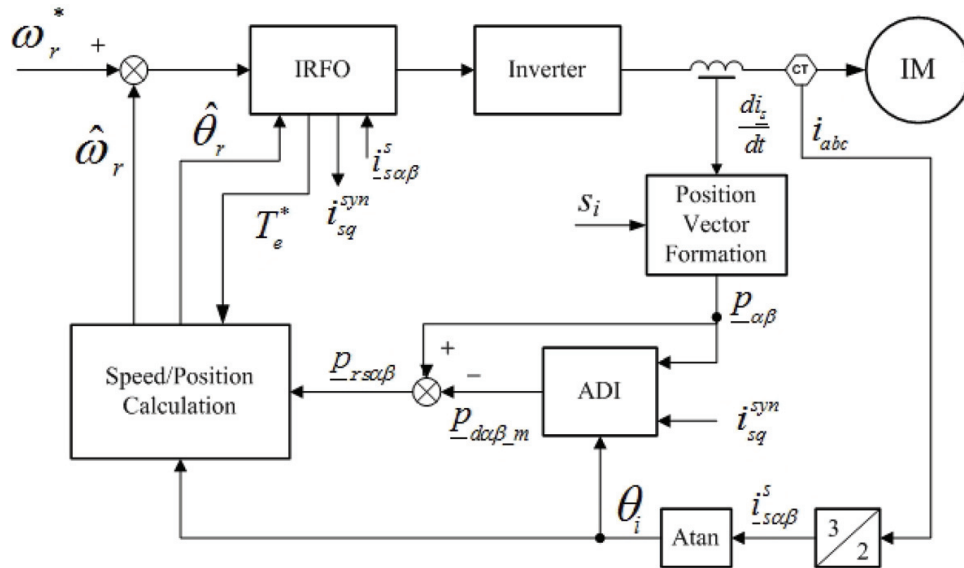


Figure 5. System schematic of the sensorless speed control (ADI).

when $S_i = 1$, Eqs. (27) and (28) can be used. Each of the other five sectors has its own set of equations like (27) and (28) such that the continuous position signal $p_{\alpha\beta}$ can be constructed. Ideally, $p_{\alpha\beta}$ can be used for position/speed estimation, but due to the presence of disturbance signals, which are mainly due to the saturation of the machine, such as the $2f_e$ and $4f_e$ components [3], the estimated position will become distorted if $p_{\alpha\beta}$ is used directly. This disturbance cannot be eliminated by filtering since the disturbance frequencies converge to the wanted signal frequencies as the excitation frequency approaches zero. As a result, a memory-type filter is required. In this work, an adaptive disturbance identifier (ADI) [17] is employed to separate these disturbance signals, i.e., $p_{d\alpha\beta_m}$ which are filtered out from $p_{\alpha\beta}$. This identifier

Machine Parameters	Values
Rated Power	30kW
Number of Poles	4
Connection	Delta
Lo,Ls	82.5mH, 83.5mH
Rotor Slot Number Nr	56 (unskewed, open slot)
Stator Slot Number	48
Rated Frequency	50 Hz

Table 2. Parameters of the IM.

does not require a pre-commissioning phase. Rather it initiates a learning type sequence in which the resolver disturbance signals are estimated and continually refined as the machine passes through the appropriate torque-speed space [17]. The $p_{d\alpha\beta_m}$ disturbance signals are stored in memory and are subtracted from the uncompensated signals to give the compensated signal $p_{rsa\beta}$. The resulting position vector $p_{rsa\beta}$ is fed to the Speed/Position Calculation block for the speed and position estimation.

The Speed/Position Calculation block further refines the position signals. Because the ADI-compensated rotor slot position still consists of a speed dependent disturbance signal rotating at $N_r\omega_r/p-2\omega_i$, which is attributed to the inter-modulation effect between the slotting and saturation in the machine [11], and can be conveniently removed by a side band filter [11]. The filtered position signal is shown in **Figure 6**.

The position signals obtained so far can be used for position acquisition in the way shown in (29). However, a mechanical observer similar to [19] is utilized to reduce the noise. The schematic is given in **Figure 7**.

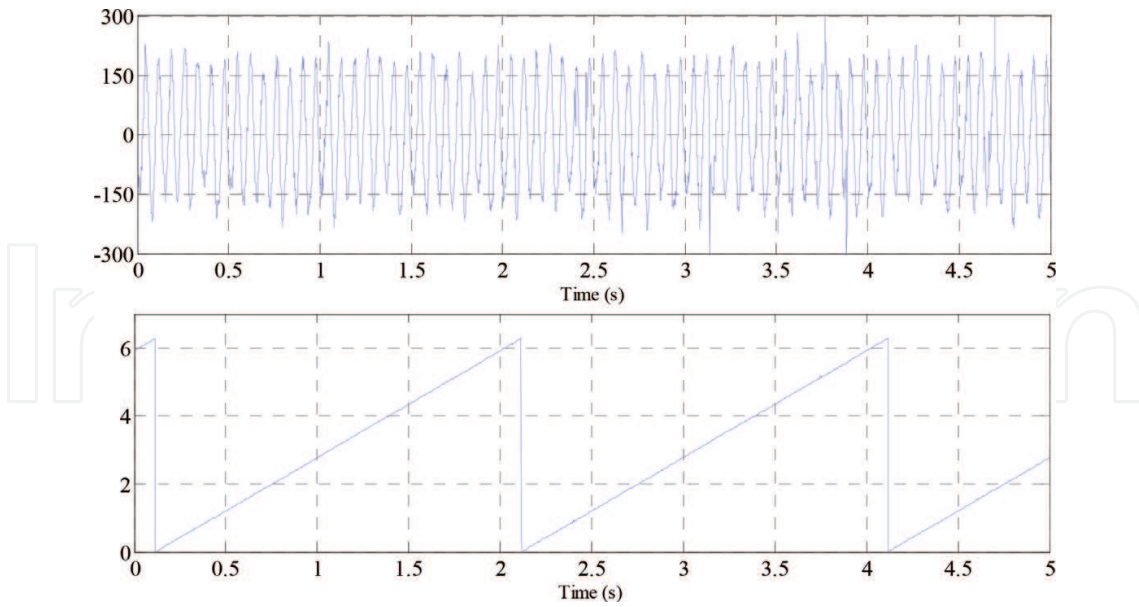


Figure 6. Position estimation at 15 rpm with 75% rated load ($f_e = 1.0$ Hz). Top: filtered position signal; and bottom: estimated rotor position (rad).

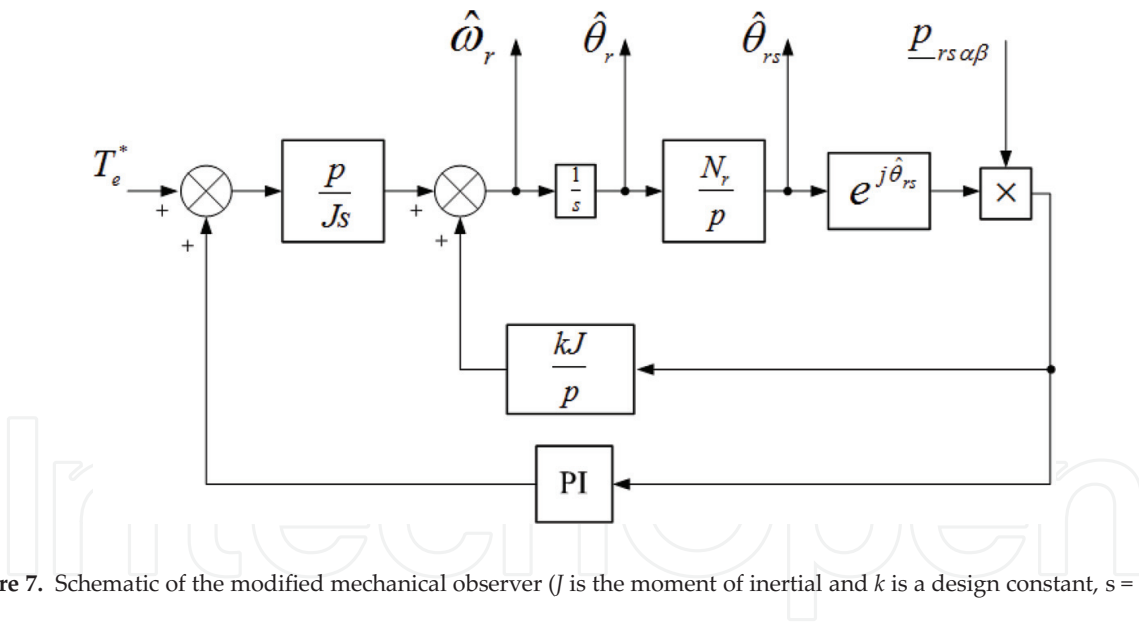


Figure 7. Schematic of the modified mechanical observer (J is the moment of inertial and k is a design constant, $s = d/dt$).

Figure 8 shows an improved estimated rotor position signal before and after the observer. An offset angle can be observed between these two rotor positions. This is due to the fact that the mechanical observer’s estimation was aligned to the encoder’s angle initially, whereas the estimate from the SBF only yields the incremental position.

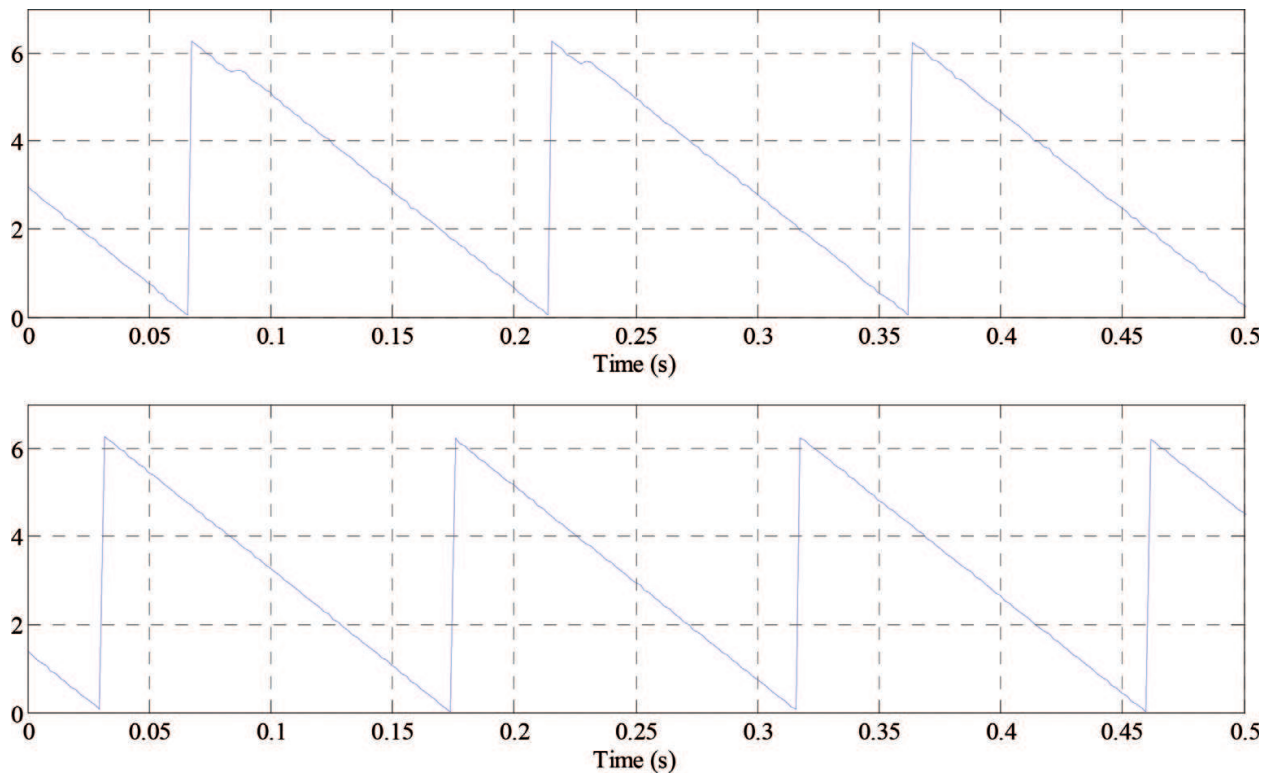


Figure 8. Rotor position estimation (rad) at -210 rpm, no load top: before the observer, bottom: after the observer.

4. Experimental results

The following experiments show the operation of the drive under sensorless speed control at low and higher speeds. The induction motor drive is under speed sensorless control. The load machine is under torque control. The rating of the dynamometer converter is such that only a loading of 80% rate can be applied to the induction motor. It is emphasized that all the experimental waveforms were recorded on an experiment rig.

Figure 9 shows that under no load condition the IM is reversed at 6 rpm, corresponding to the excitation frequency $f_e = 0.2$ Hz. Good rotor estimation can be seen. In Figure 10, the drive performs a speed reversal at ± 12 rpm under 70% rated load condition. At -12 rpm, this load condition corresponds to the drive under braking at zero excitation frequency. Since a constant torque is applied to the DC load machine, under speed reversal, the amplitude of i_{sq} changes due to the losses involved.

In Figure 11, the drive was taken between ± 210 rpm under no load. This test confirms the capability of the drive to perform larger speed transients.

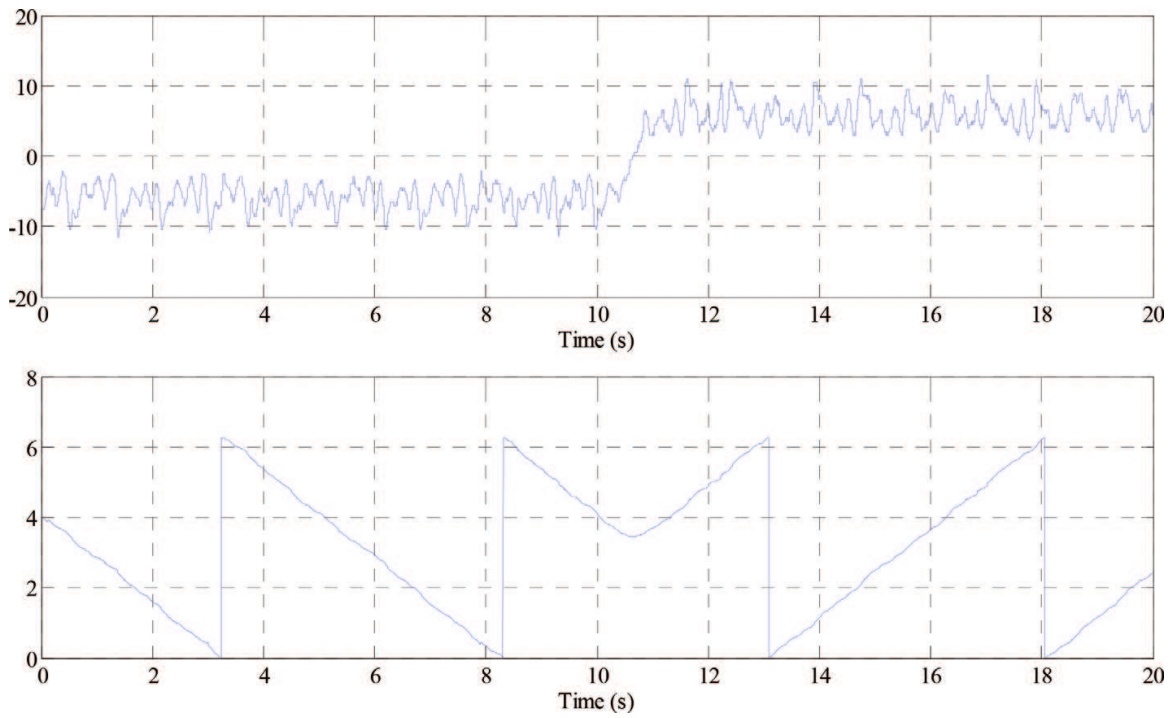


Figure 9. Speed reversal at 6 rpm, no load top: measured speed (rpm), bottom: estimated rotor position (rad).

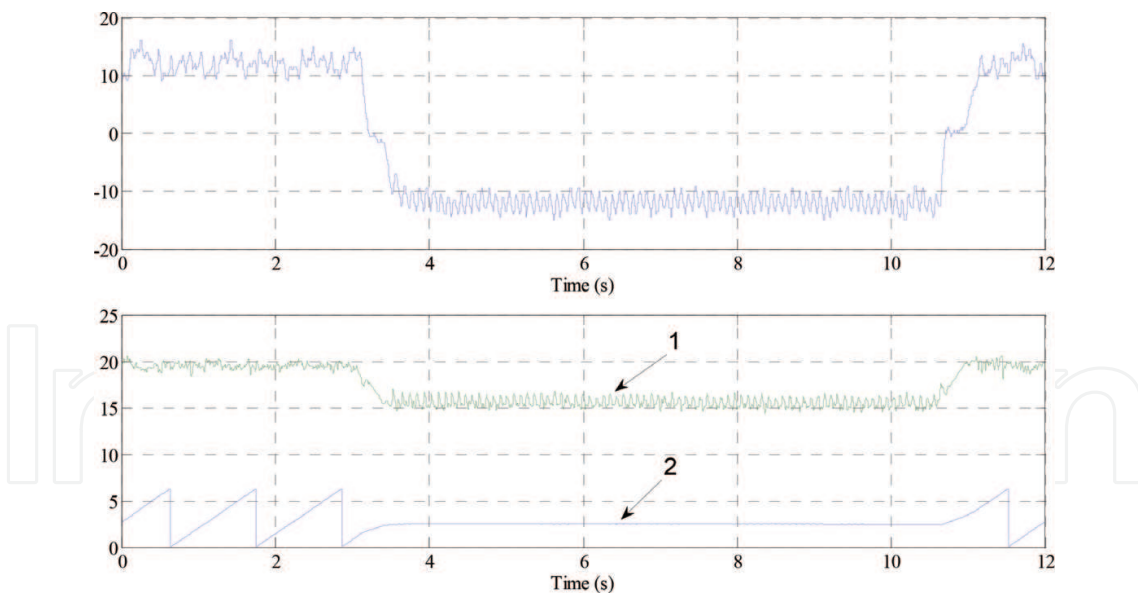


Figure 10. Speed reversal at ± 12 rpm under 70% rated load top: measured speed (rpm), bottom: rotor flux angle (1, rad) and filtered I_{sq} (2, A).

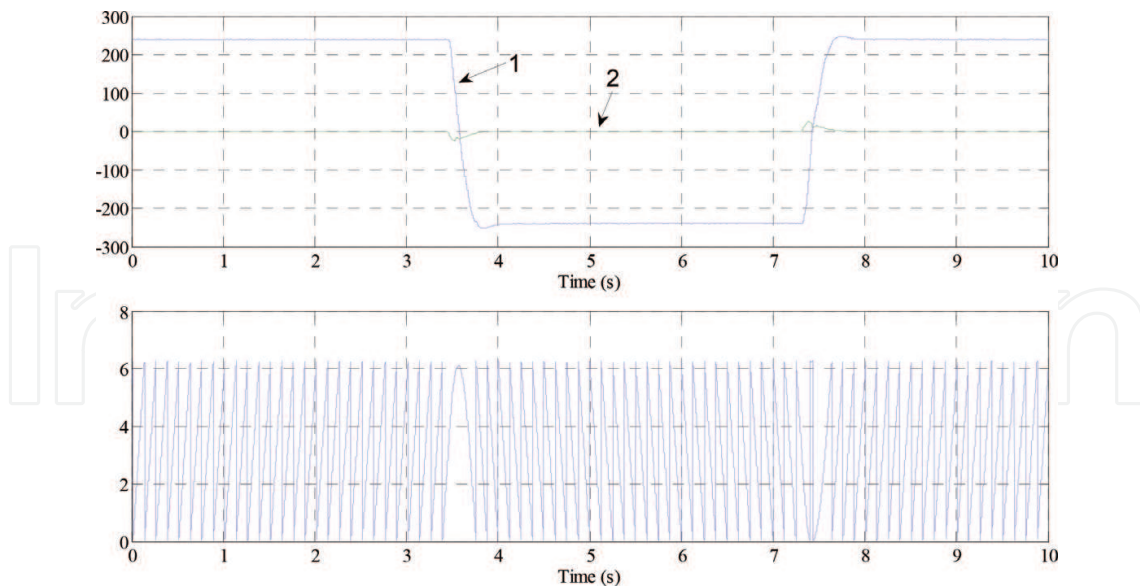


Figure 11. Speed reversal at ± 240 rpm, no load top: measured speed (1, rpm) and filtered I_{sq} (2, A); bottom: estimated rotor position (rad).

5. Conclusion

A sensorless position scheme for AC machines is presented relying on the line-current derivative measurements in response to a fundamental PWM switching sequence. The rotor position angle is derived due to the tracking of rotor slotting and the signal is used for sensorless control. If the anisotropy caused by the main flux saturation is tracked, for example, in a permanent magnet machine, this method is applicable throughout a very wide speed range. If rotor slotting is tracked, then the maximum speed is limited by the Nyquist frequency associated with the rotor slot passing frequency. In principle, however, the method can work over the entire torque-speed envelope.

Author details

Qiang Gao^{1*}, Greg Asher² and Mark Sumner²

*Address all correspondence to: gaoqiang@sjtu.edu.cn

1 Shanghai Jiao Tong University, Shanghai, China

2 University of Nottingham, Nottingham, UK

References

- [1] Jansen PL, Lorenz RD. Transducerless field orientation concepts employing saturation induced saliencies in induction machines. In: Proceedings of the IEEE IAS Annual Meeting; Nov/Dec 1995. p. 174-181
- [2] Holtz J. Sensorless position control of induction motors – An emerging technology. IEEE Transactions on Industrial Electronics. 1998;**45**(6):840-852. DOI: 10.1109/41.735327
- [3] Teske N, Asher GM, Sumner M, Bradley KJ. Encoderless position estimation for symmetric cage induction machines under loaded conditions. IEEE Transactions on Industrial Applications. 2001;**37**(6):1793-1800. DOI: 10.1109/28.968193
- [4] Silva CA, Asher GM, Sumner M, Bradley KJ. Sensorless rotor position control in a surface mounted PM machine using *HF* voltage injection. In: Proceedings of the EPE –PEMC on CD-ROM; 2002
- [5] Linke M, Kennel R, Holtz J Sensorless position control of permanent magnet synchronous machines without limitation at zero speed. In: Proceedings of the IEEE IECON 2002 on CD-ROM; 2002
- [6] Corley MJ, Lorenz RD. Rotor position and velocity estimation for a salient-pole permanent magnet synchronous machine at standstill and high speeds. IEEE Transactions on Industry Applications. 1998;**34**(4):784-789. DOI: 10.1109/28.703973
- [7] Ha JI, Sul SK. Sensorless field orientation of an induction machine by high frequency signal injection. In: Proceedings of the IEEE IAS Annual Meeting; 1997. p. 426-432
- [8] Schroedl M. Sensorless control of AC machines at low speed and standstill based on the INFORM method. In: Proceedings of the IEEE IAS Annual Meeting; 1996. p. 270-277
- [9] Caruana C, Asher GM, Clare J. Sensorless flux position estimation at low and zero frequency by measuring zero-sequence current in delta connected cage induction machines. In: Proceedings of the IEEE IAS Annual Meeting on CD-ROM; 2003
- [10] Staines CS, Asher GM, Sumner M. Sensorless control of induction machines at zero and low frequency using zero sequence currents. In: Proceedings of the IEEE IAS Annual Meeting on CD-ROM; 2004
- [11] Holtz J, Pan H. Elimination of saturation effects in sensorless position controlled induction motors. In: Proceedings of the IEEE IAS Annual Meeting on CD-ROM; 13–18 October 2002; Pittsburgh
- [12] Robeischl E, Schroedl M. Optimized INFORM measurement sequence for sensorless PM synchronous motor drives with respect to minimum current distortion. IEEE Transactions on Industrial Applications. 2004;**40**(2):591-598. DOI: 10.1109/TIA.2004.824510
- [13] Wolbank T, Machl J. A modified PWM scheme in order to obtain spatial information of ac machines without mechanical sensor. In: Proceedings of the IEEE APEC; 2002. p. 310-315

- [14] Juliet J, Holtz J. Sensorless Acquisition of the rotor position angle for induction motors with arbitrary stator windings. In: Proceedings of the IEEE IAS Annual Meeting on CD-ROM; 2004
- [15] Erdman JM, Kerkman RJ, Schlegel DW, Skibinski GL. Effect of PWM inverters on AC motor bearing currents and shaft voltages. IEEE Transactions on Industrial Applications. 1996;**32**(2):250-259. DOI: 10.1109/28.491472
- [16] Gao Q, Asher GM, Sumner M, Makyš P. Position estimation of AC machines at all frequencies using only space vector PWM based excitation. In: Proceedings of the IEEE 3rd International Conference on Power Electronics, Machines and Drives (PEMD); 2006. p. 61-70
- [17] Gao Q, Asher GM, Sumner M. Sensorless position and speed control of induction motors using high frequency injection and without off-line pre-commissioning. In: Proceedings of the 31st Annual Meeting of IEEE, IES 2005 on CD-ROM; 2005
- [18] Wolbank TM, Machl JL, Hauser H. Closed-loop compensating sensors versus new current derivative sensors for shaft-sensorless control of inverter fed induction machines. IEEE Transactions on Instrumentation and Measurement. 2004;**53**(4):1311-1315. DOI: 10.1109/TIM.2004.830561
- [19] Jansen PL, Lorenz RD. Transducerless position and velocity estimation in induction and salient AC machines. IEEE Transactions on Industry Applications. 1995;**31**(2):240-247. DOI: 10.1109/28.370269

